Uwe Schroeder, Claudia Richter, Min Hyuk Park, Tony Schenk, Milan Pešic, Michael Hoffmann, Franz P. G. Fengler, Darius Pohl, Bernd Rellinghaus, Chuanzhen Zhou, Ching-Chang Chung, Jacob L. Jones, Thomas Mikolajick

Lanthanum-Doped Hafnium Oxide: A Robust Ferroelectric Material

Erstveröffentlichung in / First published in:

Inorganic Chemistry. 2018, 57(5), S. 2752-2765 {Zugriff am: 06.09.2022}. ACS Publications. ISSN 1520-510X.

DOI: https://doi.org/10.1021/acs.inorgchem.7b03149

Final edited form was published in "Inorganic Chemistry". 2018, 57(5), S. 2752-2765. ISSN 1520-510X.
https://doi.org/10.1021/acs.inorgchem.7b03149

Lanthanum-Doped Hafnium Oxide: A Robust Ferroelectric Material

Uwe Schroeder,[*†] Claudia Richter,[†] Min Hyuk Park,[†] Tony Schenk,[†] Milan Pešić,[†] Michael Hoffmann,[†] Franz P. G. Fengler,[†] Darius Pohl,[‡] Bernd Rellinghaus,[‡] Chuanzhen Zhou,[§] Ching-Chang Chung,[§] Jacob L. Jones,[§] and Thomas Mikolajick[†//]

[†] *NaMLab gGmbH, Noethnitzer Straße 64, 01187 Dresden, Germany*
[‡] *IFW Dresden, Helmholtz Straße, Dresden, Germany*
[§] *Department of Materials Science and Engineering, North Carolina State University, Raleigh, North Carolina 27695-7907, United States*
Analytical Instrumentation Facility, College of Engineering, North Carolina State University, Raleigh, North Carolina 27695-7531, United States
[//] *Chair of Nanoelectronic Materials, TU Dresden, 01062 Dresden, Germany*

ABSTRACT: Recently simulation groups have reported the lanthanide series elements as the dopants that have the strongest effect on the stabilization of the ferroelectric non centrosymmetric orthorhombic phase in hafnium oxide. This finding confirms experimental results for lanthanum and gadolinium showing the highest remanent polarization values of all hafnia based ferroelectric films until now. However, no comprehensive overview that links structural properties to the electrical performance of the films in detail is available for lanthanide doped hafnia. La:HfO_2 appears to be a material with a broad window of process parameters, and accordingly, by optimization of the La content in the layer, it is possible to improve the performance of the material significantly. Variations of the La concentration leads to changes in the crystallographic structure in the bulk of the films and at the interfaces to the electrode materials, which impacts the spontaneous polarization, internal bias fields, and with this the field cycling behavior of the capacitor structure. Characterization results are compared to other dopants like Si, Al, and Gd to validate the advantages of the material in applications such as semiconductor memory devices.

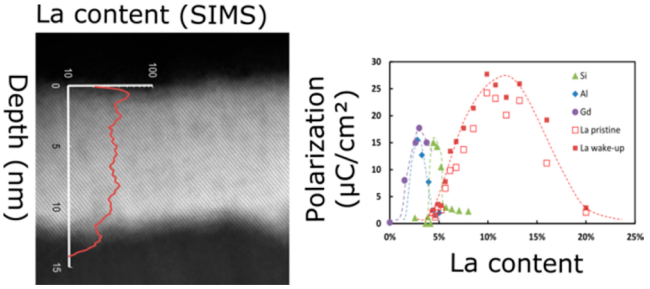

1. INTRODUCTION

For material scientists, the new class of inorganic HfO_2 based ferroelectrics are of special interest, because they are lead free, simple binary oxides, and exhibit a nonperovskite structure with a remarkably low relative permittivity (~20−30) compared to ~300 or greater permittivity of conventional ferroelectrics like $Pb(Ti,Zr)O_3$.[1] Since the discovery of ferroelectricity in doped HfO_2,[2] a variety of different dopants (e.g., Si,[3] Al,[4] Y,[5] Gd,[6] La,[7] Sr[8]) have been examined to discover the dopant material with best properties for applications in semiconductor, piezo , and pyroelectric devices. Dopants with an ionic radius smaller than Hf typically showed ferroelectric and anti ferroelectric charac teristics in a narrow dopant range. Larger dopants exhibited only ferroelectric behavior but have a wider process window.[9] The polar orthorhombic phase ($Pca2_1$) was suggested as the origin of the ferroelectric properties.[2,10] Nonetheless, there is a substantial mismatch between the exciting material aspects of this new ferroelectric together with the proven application potential on one hand and the significant lack of basic studies on how to influence material properties and perturbing effects on the other hand. Lanthanum doped HfO_2 is the perfect example to highlight this point. Simulation groups[11] reported that the lanthanide series elements (in addition to other dopants: Ca, Sr, Ba) are the dopants in hafnium oxide that have the strongest effect on the stabilization of the ferroelectric non centrosymmetric orthorhombic phase. This result is confirmed by first experimental results for lanthanum and gadolinium showing the highest remanent polarization values of all hafnia based ferroelectric films reported so far (P_r > 30 $\mu C/cm^2$),[13] good endurance properties (1 × 10^9 field cycles without fatigue), and complementary metal oxide semiconductor (CMOS) back end compatibility for low La concentrations.[12] While initially reported P_r values of 45 $\mu C/cm^2$[13] could not be reproduced in later studies,[12,14] values similar or higher compared to other dopants have been consistently achieved. However, a comprehensive overview that links structural properties to the electrical performance of the films in detail is still missing for this important class of larger dopants. La Doped HfO_2 appears to be a material with a broad process

Final edited form was published in "Inorganic Chemistry". 2018, 57(5), S. 2752-2765. ISSN 1520-510X.
https://doi.org/10.1021/acs.inorgchem.7b03149

window with respect to doping concentration, and accordingly, by optimization of the La content in the layer, it is possible to improve the performance of the material significantly. Because of this broad process window, a detailed and robust study of the impact of different dopant contents on the ferroelectric properties can be performed. The resulting changes in the crystallographic structure in the bulk of the films and at the interfaces to the electrode materials can impact the spontaneous polarization, internal bias fields, and with this the field cycling behavior of the capacitor structure. By putting these results into perspective of results obtained with other dopants in previous studies, new insight into the general issue of stabilizing the ferroelectric phase in doped hafnia is developed.

Therefore, to gain new understandings, this study focuses on the detailed characterization of La doped HfO_2 films with fine steps in a much broader La concentration range compared to previous studies.[12−14] Results of structural characterization methods (electron microscopy, X ray diffraction, secondary ion mass spectrometry) are very well correlated with the electrical properties. A close comparison of different dopants, especially the difference between Si as a dopant with smaller atomic radius resulting in a fragile ferroelectric material[3] and La as a larger dopant resulting in a robust ferroelectric phase, is performed to gain more insights into the root causes for ferroelectricity in HfO_2.

2. EXPERIMENTAL SECTION

For electrical characterization, the La:HfO_2 films were integrated in a capacitor structure ref 3 with 12 nm thick titanium nitride bottom and top electrodes sputtered in a BESTEC physical vapor deposition (PVD) tool at room temperature. The capacitor areas were defined by evaporating 10 nm of titanium and 25 nm of platinum through a shadow mask and etching the titanium nitride top electrode afterward in a diluted standard clean 1 ($H_2O/H_2O_2/NH_4OH$ in a ratio of 50:2:1 at 50 °C). Lanthanum doped hafnium oxide films were deposited in an Oxford Instruments OpAL ALD tool by atomic layer deposition (ALD). Tetrakis[ethylmethylamino]hafnium (TEMAHf, $Hf(N(CH_3)(C_2H_5))_4$) and tris(isopropyl cyclopentadienyl)lanthanum ($La(iPrCp)_3$) were chosen as metalorganic precursors. Previous results[15] showed that HfO_2 deposited with H_2O as the oxygen source yields the best electrical properties compared to other oxygen sources, and it was therefore chosen for this work. La_2O_3 ALD deposition is impacted by the low volatility and decomposition temperature of the La precursor,[16] which usually results in lower film quality of the deposited films. To improve the film properties, an inductively coupled O_2 plasma was used for La_2O_3 deposition. Similar samples were processed in comparison with an H_2O precursor for La_2O_3 deposition, but lower remanent polarization and endurance results were observed. For all processes, the deposition temperature was held at 280 °C. The growth rate of the pure HfO_2 and La_2O_3 ALD processes were determined as 0.11 and 0.09 nm/cycle, respectively. The films were doped by replacing single HfO_2 cycles by La_2O_3 cycles, which allows the adjustment of the La content by varying the ratio of HfO_2 cycles to La_2O_3 cycles. In this study cycle ratios in the range between 1:1 and 30:1 were investigated. The absolute number of ALD cycles defines the thickness of the film. Here, we focused mainly on samples with a thickness of 10−15 nm. All dielectric films were amorphous after deposition, requiring a crystallization anneal to achieve ferroelectric behavior, which was performed in an AST rapid thermal processing tool under N_2 atmosphere for typically 20 s. To find the optimum annealing conditions, the temperature was varied from 600 to 1000 °C.

For structural film analysis, a Bruker D8 Discover X ray diffraction (XRD) tool (Cu Kα radiation: 0.154 nm wavelength) was used to determine the crystallographic structure in addition to film thickness and density by X ray reflectometry (XRR). Rietveld refinements of the diffraction patterns were utilized to estimate the different phase fractions in the thin films and were performed using TOPAS software by Bruker (as described in more detail elsewhere[17]). Furthermore, time of flight secondary ion mass spectrometry (TOF SIMS) analyses were performed using a TOF SIMS V (ION TOF, Inc.) tool to investigate the lanthanum distribution within the HfO_2 films. Lamellas were prepared for scanning transmission electron microscopy (STEM) using a focused ion beam for sample preparation and a C_S probe corrected Titan[3] 80−300 for STEM imaging (for details see ref 3). Ferroelectric properties including remanent polarization P_r, coercive field E_c, small signal capacitance (to extract the relative permittivity k), and field cycling endurance were measured on the capacitors with an AixACCT TFA3000 ferroelectric tester. P E hysteresis loops were performed at 1 kHz using a triangular voltage signal. Electric field cycling to verify endurance and breakdown behavior was performed using a frequency of 100 kHz with rectangular voltage pulses typically at 4 MV/cm. First order reversal curve measurements were performed on a Keithley 4200 SCS with pulse measurement units using a constant voltage ramp rate of 0.32 V/μs.

3. RESULTS

3.1. Anneal Study. Various dopants in HfO_2 result in a different crystallization temperature depending on the dopant content and the thickness of the doped HfO_2 film.[18] Accordingly, an anneal study is important to find the optimal parameters to form the ferroelectric phase in doped HfO_2. Figure 1 shows the impact of annealing on the remanent

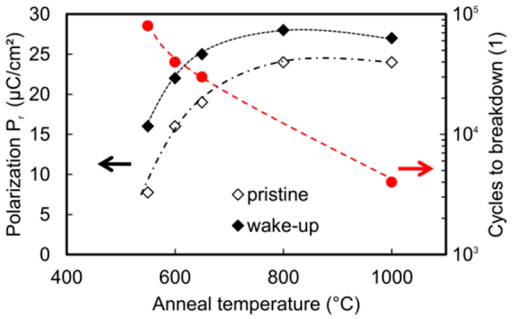

Figure 1. Remanent polarization P_r vs anneal temperature for a pristine sample in comparison to a sample after wake up (black curves, left axis). Number of triangular field cycles at 4.2 MV/cm and 100 kHz to reach breakdown as a function of the anneal temperature (red curve, right axis). Lines are a guide.

polarization of a capacitor structure with a 12 nm La:HfO_2 (1:10 La/Hf ALD cycle ratio resulting in ~10 cat% La in HfO_2) dielectric in a temperature range from 550 to 800 °C for 20 s and 1000 °C for 1 s in N_2 ambient. This increase of annealing temperature results in an enhancement of the remanent polarization from 8 to 24 μC/cm^2 for the pristine sample and from 16 to 28 μC/cm^2 after ~1 × 10^4 field cycles at 4.2 MV/cm. The maximum polarization value at 800 °C was slightly reduced to 27 μC/cm^2 after annealing at 1000 °C. This decrease in the maximum remanent polarization for temperatures higher than 800 °C can be explained by a higher nonpolar monoclinic phase portion as discussed in the Supporting Information (Figure SI 1). Additionally, for higher annealing temperatures, the number of cycles to breakdown decreased due to defect diffusion of Ti and N into the HfO_2 and O diffusion into the TiN electrodes forming TiO_x leaving an oxygen deficient interfacial HfO_x layer behind[22,23,43](see TOFSIMS results in Figure SI 5). Since the main focus of the paper was to characterize the ferroelectric (FE) properties of

Final edited form was published in "Inorganic Chemistry". 2018, 57(5), S. 2752-2765. ISSN 1520-510X.
https://doi.org/10.1021/acs.inorgchem.7b03149

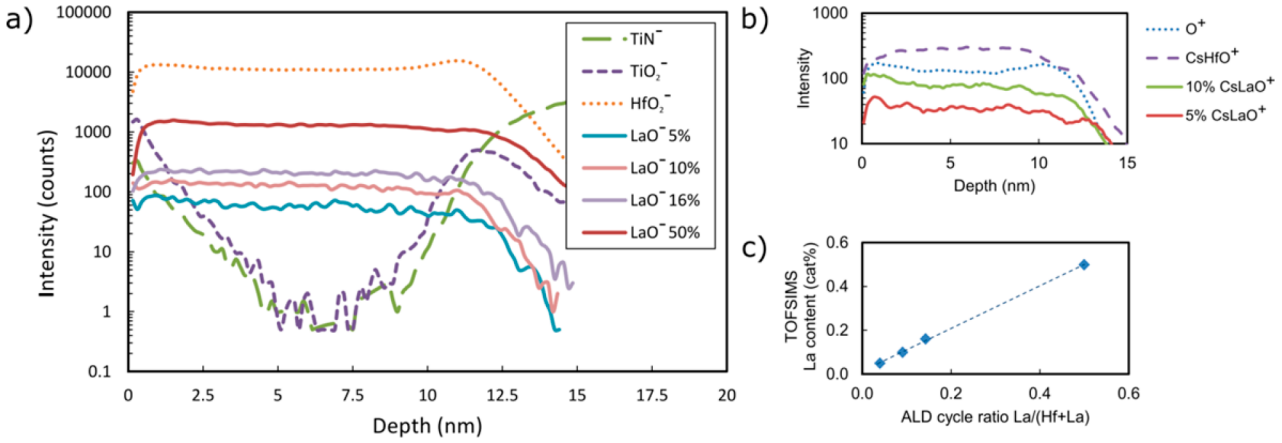

Figure 2. (a) TOF SIMS results in negative ion mode for samples with different La content ranging from 5 to 50 cat%. (b) TOF SIMS results in positive ion mode for a sample with 5 and 10 cat% La content. (c) TOF SIMS La content as a function of ALD cycle ratio.

the HfO_2 layer, the anneal condition reaching the highest remanent polarization value without increasing the leakage current beyond 1×10^{-6} A/cm^2 at 1 V (to a level, where the leakage current impacts the shape of the hysteresis loop) was chosen (800 °C 20 s) for further experiments. Optimization of the capacitor stack for memory applications would lead to a different assessment of optimal annealing temperature. Since memory capacitors are formed in a back end of line (BEOL) process, the thermal budget would need to be decreased as much as possible and typically would need to be in the temperature range from 400 to 500 °C.[19] To achieve this target, Kozodaev et al. revealed that a reduction of the La content would further decrease the crystallization temperature at reasonable polarization values.[12] Besides La:HfO_2, $Hf_xZr_{1-x}O_2$ or Gd:HfO_2 were shown to exhibit ferroelectricity at such low annealing temperatures.[20,21]

3.2. Structural Characterization. La doped HfO_2 films are deposited within a TiN/14 nm La:HfO_2/TiN capacitor structure using a variety of different ALD Hf/La super cycling ratios from 30:1 to 1:1. TOF SIMS characterization is performed on a selection of these film stacks to determine the material composition changes within the structure. Here, the La composition in the dielectric layer after annealing at 800 °C for 20 s in N_2 was the main interest as discussed in the previous section. An almost uniform LaO_x content in the HfO_2 bulk is visible as shown in Figure 2a. Plotting the resulting La content as a function of the ALD cycle ratio results in a linear relationship with a slope of 1.01 indicating a very similar growth rate and comparable growth behavior of LaO_x with increasing HfO_2 thickness (Figure 2c). These results fit nicely to the comparable growth rate of both films as determined for the pure LaO_x and HfO_2 growth (0.09 nm/cycle for La_2O_3 and 0.11 nm/cycle for HfO_2).

With a closer look at the composition close to the electrode interfaces, the following observations can be made. A thin TiO_x interlayer is formed at the interface between the TiN electrode and the La:HfO_2 due to an interface reaction during the crystallization anneal.[22,23] Furthermore, a higher HfO_2^- intensity is visible at the interface between the TiN electrode and La:HfO_2 for all measured samples (Figure 2a only shown for one sample). In general, secondary ion yield of many species in SIMS experiments can be enhanced by O content and other carbon containing contaminations at the interface, which do not reflect their true concentration. To elucidate this, positive ion depth profiles of cesium molecular cluster ions CsM^+ can be used.[24] Here, Cs^+ is the ion use for sputtering, which is implanted during sputtering and can form Cs molecular species. Typically, the intensity of the CsM^+ signal is not or is less affected by oxygen or other contamination in the material. Therefore, the positive $CsHfO^+$ is more reliable (Figure 2b). Overall, a similar O_2 enhancement to HfO_2^- signal is detected at the interface of La:HfO_2 to both TiN electrodes. Furthermore, within the doped HfO_2 bulk region the Hf/La ratio is very uniform for La contents greater than 5 cat% in positive and negative ion modes. Below 5 cat%, a La content modulation is visible in positive ion mode as expected from the ALD La/Hf supercycle processing. Five La intensity maxima are present, which fit to five La_2O_3 supercycles in 140 HfO_2 ALD cycles. For La concentrations above 5 cat% the TOF SIMS resolution of ~2 nm is not sufficient to observe these supercycles. Dopant modulations are also reported for a Si:HfO_2 layer.[3] In the first three nanometers from the top electrode it appears that a Hf deficient and La enriched region is present, which might be related to a Cs initial sputtering effect.

Figure 3a shows the grazing incidence X ray diffraction (GIXRD) patterns of 14 nm thick La:HfO_2 thin films with various La doping concentrations annealed at 800 °C for 20 s. For the case of a pure HfO_2 thin film, the crystalline phase is typically the monoclinic phase. For 6 cat% La doping, the relative fraction of the monoclinic phase significantly decreases, and strong diffraction peaks from the orthorhombic or cubic phase can be clearly observed. Derived from the diffraction peak split at a 2θ angle of ~51°, the crystalline phase should have a certain orthorhombic phase fraction. Although a sharp diffraction peak from the Si substrate could be also observed for some of the diffraction patterns, the rather broad shape of diffraction peak clearly implies the existence of the orthorhombic phase. This 2θ value of ~51° refers to the location of orthorhombic 220 and 022 diffraction peaks.[2,35] This peak was suggested as one important indication of the orthorhombic phase in a previous study.[2,35] With further increasing La content toward 10 cat%, the intensity of the diffraction peaks from the monoclinic phase further decreases, and the dominant crystalline phase is believed to be the orthorhombic one. For the La doping concentration of 13 cat%, monoclinic diffraction peaks cannot be observed anymore, and the locations of diffraction peaks are shifted compared to the 10

Final edited form was published in "Inorganic Chemistry". 2018, 57(5), S. 2752-2765. ISSN 1520-510X.
https://doi.org/10.1021/acs.inorgchem.7b03149

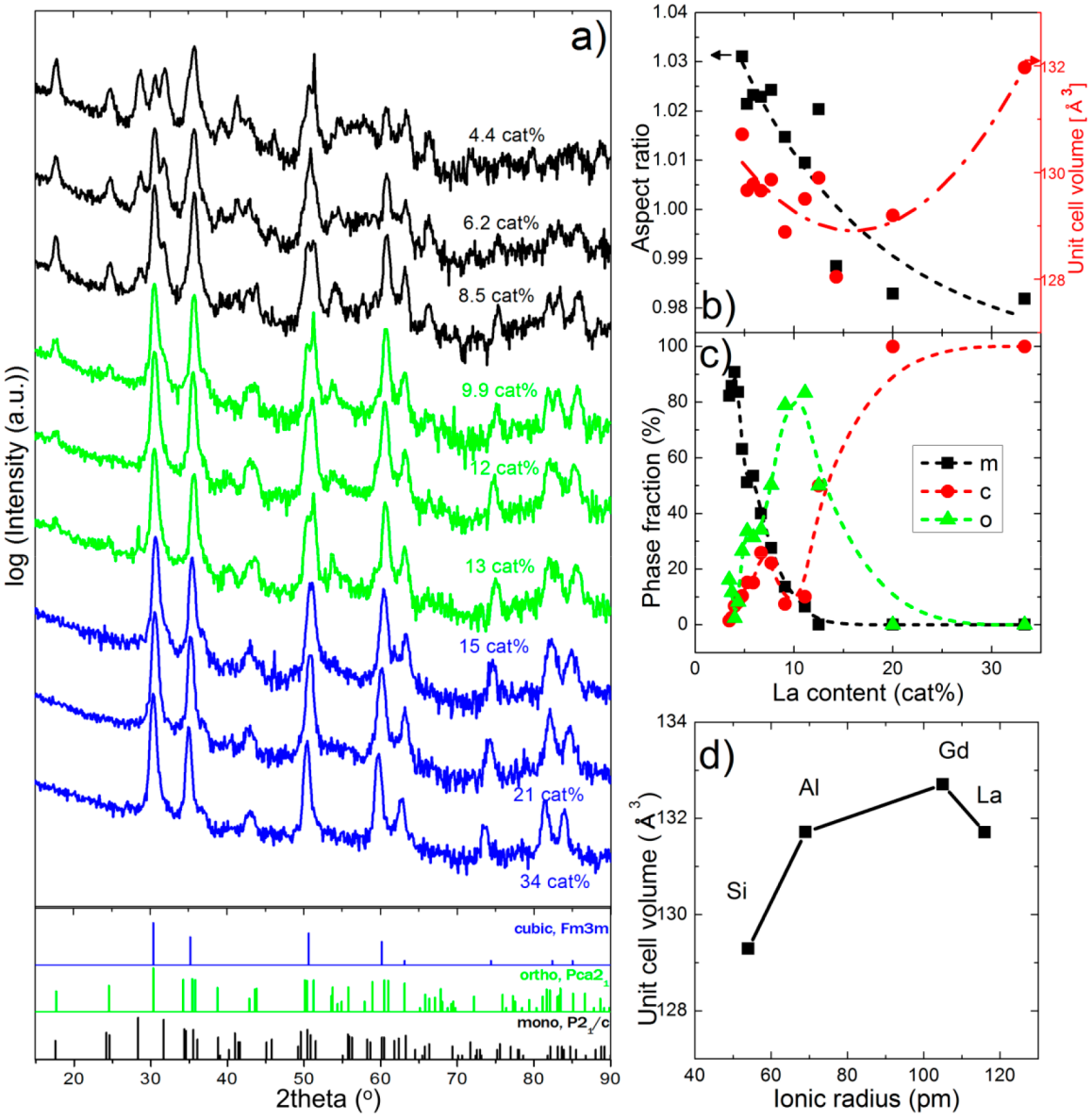

Figure 3. (a) GIXRD patterns for La doped HfO_2 annealed at 800 °C for 20 s. (b) Aspect ratio $(2a/(b + c)$ for the orthorhombic phase of the unit cell and the unit cell volume as a function of the La content. (c) Relative phase fractions as determined by refinement of GIXRD patterns from Figure 3a. (d) Unit cell volume of the orthorhombic phase for Si, Al, Gd, and La doping in HfO_2 as a function of ionic radius for the dopant concentration with the highest orthorhombic phase fraction. Lines are a guide.

cat% doped film. The 100 and 110 diffraction peaks at 18 and 25° can be observed up to 13 cat% La doped HfO_2 film, but they cannot be detected when the La content increases beyond 15 cat%. These peaks can be observed for the monoclinic and the orthorhombic phase, but they are forbidden for the tetragonal and the cubic phase. Such changes can be attributed to the transition from the orthorhombic to the cubic phase. Shimizu et al.[25] reported that the 110 diffraction peak at 18° disappeared when the dominant crystalline phase of epitaxial Y doped HfO_2 film changes from the orthorhombic to the tetragonal phase with increasing Y content. Within the GIXRD pattern of the 20 cat% doped film, the split of diffraction peaks at 51° disappears, suggesting that the predominant crystalline phase is the cubic phase. Moreover, only two cubic diffraction peaks could be observed within the 2θ range of 80−90°, which can be clearly distinguished from the tetragonal, orthorhombic, or monoclinic phase. The GIXRD pattern of the 30 cat% sample also shows the typical pattern of the cubic phase; thus, it is concluded that La doping is stabilizing the cubic phase when the dopant concentration is higher than 20 cat%.

In our previous study, we suggested that the change of unit cell parameters, which can be calculated from the diffraction peak locations, can provide useful information to estimate the crystalline phase in doped HfO_2 thin films.[17] Especially, the aspect ratio $2a/(b + c)$ for the orthorhombic phase and c/a for the tetragonal phase are strongly coupled to the change of the crystalline phase and resulting electrical properties.[17] The aspect ratio of the orthorhombic phase was larger than 1.02, but it decreased below 1.0 when the doping concentration increased, which resulted in a phase evolution toward the tetragonal phase.[17] Figure 3b shows the change of the aspect ratio and unit cell volume for the La:HfO_2 samples doped with more than 5 cat% doping concentration. For the samples with a doping concentration lower than 5 cat%, the dominant

Final edited form was published in "Inorganic Chemistry". 2018, 57(5), S. 2752-2765. ISSN 1520-510X.
https://doi.org/10.1021/acs.inorgchem.7b03149

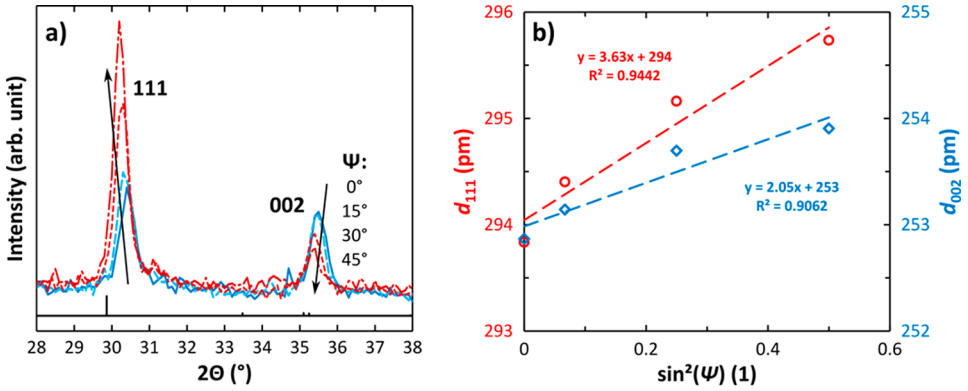

Figure 4. (a) XRD results for a 20 nm thick La:HfO_2 sample with 10 cat% La annealed at 800 °C for 20 s measured in Bragg−Brentano geometry for different angles Ψ (angle between surface normal and scattering vector). The reference pattern of the orthorhombic phase is added below in black (PDF No. 04 005 5597). The intensity of the 002 peak, which represents the polar axis of the ferroelectric unit cell, decreases for increasing Ψ, while that of the 111 peak increases. This gives evidence for a prominent 002 texture, which is favorable to achieve a high P_r value. (b) Peak shift as a function of $\sin^2(\Psi)$ to extract internal strain. Any nonlinearity indicates that the stress is more complex than just a simple uni or biaxial stress state, which is another result of the $\sin^2(\Psi)$ method[31,32]

crystalline phase was the monoclinic phase; thus, the aspect ratio was not calculated. For a La content of 5 cat%, the aspect ratio is 1.03, which is believed to be associated with the dominant orthorhombic phase. With increasing La doping concentration from 5 to 13 cat%, the aspect ratio decreases reaching a value of 1.02 at the highest orthorhombic phase content of 10 cat%. At 13 cat% La doping, the aspect ratio becomes even smaller than 0.99, and with further increasing La content the aspect ratio saturates. The aspect ratio of 0.99 is smaller than the ideal one for the cubic phase (1.00). This observation can be attributed to in plane tensile stress, which was reported for atomic layer deposited ferroelectric Si doped HfO_2 and $Hf_{0.5}Zr_{0.5}O_2$ thin films.[18,26] The aspect ratio smaller than 1 in Si , Al , and Gd doped HfO_2 thin films in Park et al.'s previous study[17] might also originate from the effect of tensile stress. The stress in the La doped HfO_2 thin films will be discussed in more detail in Figure 4 and the related text. The change of the unit cell volume also shows an interesting dependence on the La content. The unit cell volume of the orthorhombic (or cubic phase) portions decreases with increasing La content up to the doping concentration of 14%. It increases with further increasing La content up to 33 cat%. As previously mentioned, the GIXRD patterns of 20 and 33 cat% La doped films show only diffraction peaks from the cubic phase instead of the tetragonal phase, as it was considered for other doped HfO_2 thin film in Park et al.'s previous study.[17] Therefore, the cubic phase will be referred to as the dominant phase for highly La doped HfO_2 thin films in the following text. This result agrees on one hand with theoretical predictions that dopants larger than Hf generally stabilize the cubic phase instead of the tetragonal phase,[27] but on the other hand, it is different from what is seen in bulk materials that are not subject to size, strain, or interface effects. In bulk counterparts, it is expected that a $La_2Hf_2O_7$ secondary phase is formed at these concentrations.[28,29]

In the present work, there was no evidence of this secondary $La_2Hf_2O_7$ phase in XRD and moreover not in the TEM study, which is discussed in the later part of this section. The ionic radius of La^{3+} (116 pm) is by 40% larger than that of Hf^{4+} (83 pm);[30] therefore, the lattice parameters and the interplanar distances are expected to increase for higher La doping concentration. Thus, the unit cell volume is assumed to enhance due to the larger dopant size. However, the unit cell volume decreases within increasing La doping concentration in the range from 5 to 14 cat%, which cannot be understood from a dopant size effect. This unexpected trend may be attributed to the proximity to the phase transition from the orthorhombic to the cubic or tetragonal phase with increasing doping concentration, since the unit cell volume of the cubic or tetragonal phase is smaller than that of the orthorhombic phase.[17] From the GIXRD patterns in Figure 3a and the aspect ratio changes in Figure 3b, it can be noticed that various crystalline phases such as monoclinic, orthorhombic, and cubic phases are mixed in our polycrystalline films. To quantitatively analyze the phase fractions in La:HfO_2 thin films, Rietveld refinement was conducted on the GIXRD patterns. The details of the Rietveld refinement can be found in our previous reports and the experimental section of the present work.[17] Best refinement results are reached when a texture in the 111 and 002 directions is assumed and incorporated into the model. Figure 3c summarizes the change of relative fractions of each phase as a function of La doping concentration. When the La content is less than 5 cat%, the monoclinic phase fraction is larger than 80%, and the summation of relative fractions of orthorhombic and cubic phases is less than 20%. On the one hand, when the La doping concentration increases from 5 to 13 cat% the relative fraction of monoclinic phase strongly decreases. On the other hand, the orthorhombic phase fraction enhances from 26 to 83% with increasing La content from 5 to 11 cat%. This is the highest orthorhombic phase content reached compared to various other dopants.[17] With further enlarging La concentration from 11 to 20 cat%, the cubic phase fraction increases from 10 to 100%. To summarize, the dominant crystalline phase changes from the monoclinic to the orthorhombic to the cubic phase with increasing La doping concentration. This trend is well matched with our previous observations in Si:, Al:, and Gd:HfO_2 thin films. Figure 3d shows the change of unit cell volume of the orthorhombic phase in HfO_2 thin films doped with Si, Al, Gd, and La. The data for Si:, Al:, and Gd:HfO_2 were taken from our previous report.[17] For higher dopant radius, the unit cell volume increases, except for La:HfO_2, where the unit cell volume is slightly smaller compared to Gd:HfO_2.

Final edited form was published in "Inorganic Chemistry". 2018, 57(5), S. 2752-2765. ISSN 1520-510X.
https://doi.org/10.1021/acs.inorgchem.7b03149

For the macroscopically effective values of P_r and E_c, the texture of the thin film, that is, a preferential orientation of the grains, plays an important role. As La:HfO_2 shows quite promising electrical characteristics, the question arises whether this might be related to a favorable texture. With Bragg–Brentano instead of grazing incidence geometry, the scattering vectors of all crystallographic planes that contribute to the signal in the diffractogram have the same direction. Thus, comparing the resulting intensity ratios to the reference pattern of the powder diffraction file (PDF) allows conclusions on the texture of the film.

Figure 4 shows nearly the same intensities for the 111 and the 002 peaks, which is not the case for the reference pattern. Moreover, when tilting the scattering vector away from the sample normal by increasing the angle Ψ of the goniometer, the intensity of the 002 peak decreases, while it increases for the 111 peak. This gives evidence of a comparably prominent 002 fiber like (uniaxial) texture along the substrate normal direction. Moreover, the peak positions in Figure 4a allow the analysis of the residual strain in the films via the $\sin^2(\Psi)$ method.[31,32] The corresponding analysis of the 111 and 002 peaks is shown in Figure 4b. From the (extrapolated) d_{hkl} values at $\sin^2(0°) = 0$ and $\sin^2(90°) = 1$, the interplanar distances for out of and in plane directions can be obtained. Out of plane interplanar distances of d_{111} = 294 pm and d_{002} = 253 pm are found, while their in plane counterparts are larger by 1.2% and 0.8%, respectively. The corresponding in plane stress can be estimated based on some assumptions. First, we assume Young's modulus of 284 GPa and Poisson ratio of 0.3, as reported in ref 33. For the calculation of in plane stress, we further set the out of plane component of strain as zero to make a simplified calculation for in plane stress. In reality, there is a finite out of plane strain, since the loading condition is plane stress. Under these assumptions, we determine ∼2 GPa of tensile stress for the in plane directions. Though only an estimate for the order of magnitude of the stress effect, it reveals the large values of stresses that are apparent in the films. A more rigorous treatment of the stress state would account for the nonzero, out of plane strain, though it would also require a stress free reference lattice constant as was shown by Nino et al.[34] With a stress free reference state, the hydrostatic component of strain can also be extracted. Unfortunately, identifying a stress free reference for orthorhombic HfO_2 is not straightforward, since powders that are typically used as references are in the monoclinic phase for HfO_2. This large internal stress amplitude is thought to be the reason for the low aspect ratio and increasing unit cell volume for high La contents. The reason for the different strain values calculated from the 111 and 002 diffraction peaks may be attributed to the crystal's elastic anisotropy. Furthermore, for the case of the 002 peak, there might be an overlap of diffraction peaks from 200, 020, and 002, and effects of the orientation dependence of Young's modulus or the effects of film texture are not clearly understood yet. Thus, it is believed that the strain estimated from the 111 diffraction peak is more reliable.

Of the whole sample set, the films with 10 and 16 cat% La content were chosen for a more detailed structural analysis by transmission electron microscopy (TEM). According to Figures 3c and 6c, the 10 cat% sample has the highest remanent polarization and highest orthorhombic phase fraction with some monoclinic portions. The orthorhombic phase is clearly verified (see also ref 10) within the layer (Figure 5a) with a uniform lattice structure from one TiN electrode to the other.

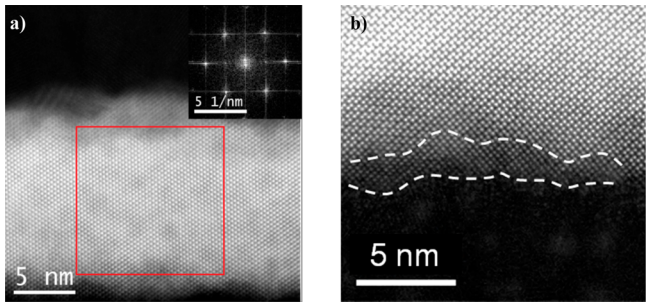

Figure 5. Orthorhombic HfO_2 of the 10 cat% La (a) with [101] zone and (b) relaxation of the orthorhombic bulk HfO_2 phase at the interface to the TiN electrode.

Other images show a monoclinic [011] or orthorhombic [101] zone (Figure SI 6b) or a [001] zone, which could be orthorhombic or monocline. Even though amorphous HfO_2 is deposited on a polycrystalline TiN bottom electrode with a 5–10 nm grain radius,[22] which is covered by a similar TiN top electrode, the La:HfO_2 crystallizes after an anneal in a granular structure with uniform lattice that is typically much larger than the TiN grains. The typical La:HfO_2 grain radius is determined by top view SEM to be 30 ± 20 nm (Figure SI 3).

As expected from the GIXRD results, mainly the orthorhombic $Pca2_1$ and some $P2_1/c$ monoclinic phase portions were identified. For the higher La content of 16 cat% only the orthorhombic phase is determined by TEM (Figure SI 7). Here, an additional cubic phase fraction is expected from GIXRD, which might be difficult to detect due to low statistics of the TEM method and due to the similarities of both phases for lower indexed lattice planes. For Gd:HfO_2 a tetragonal phase was detected at the interface between orthorhombic grains and the TiN electrode, which might stem from a crystallization of the HfO_2 at 800 °C into the t phase. During cooling, a transformation into the orthorhombic phase occurs below Curie temperature[35] in the bulk HfO_2 and only interfacial regions to TiN keep the tetragonal phase. Similar effects could also be verified for La:HfO_2. Here, some relaxation of the orthorhombic grains is present at the TiN electrode interface (Figure 5b). Furthermore, for Gd:HfO_2 an orientation relation is determined between HfO_2 and some of the TiN grains, which again could be confirmed for a small La:HfO_2 region within the statistics of the TEM analysis (Figure SI 6). One explanation for this orientation relationship could be a crystallization nucleation of the HfO_2 on some of the already crystalline TiN grains. Here, a local epitaxial growth of {111} oriented HfO_2 grains on {001} oriented TiN could be verified by XRD for Gd:HfO_2.[36] In the La case, HfO_2 grains have a 2× larger grain radius compared to Gd doping, and the location of the local epitaxy is more difficult to determine in TEM. Typical angles between TiN and HfO_2 lattice planes are shown in Figure SI 6, and a local epitaxial growth can be found in the center of the TEM image.

3.3. Electrical Characterization. In a next step, an electrical characterization of the ferroelectric capacitor is performed. First, the leakage current behavior of the capacitor structure is determined. For all samples a current of 0.5–1 $\mu A/cm^2$ at 1 V bias is monitored, which enabled further proper polarization measurements. Furthermore, no relevant leakage current change is observed within the characterized dopant range that could be related to structural differences of the material. In addition, the remanent polarization P_r is measured

Final edited form was published in "Inorganic Chemistry". 2018, 57(5), S. 2752-2765. ISSN 1520-510X.
https://doi.org/10.1021/acs.inorgchem.7b03149

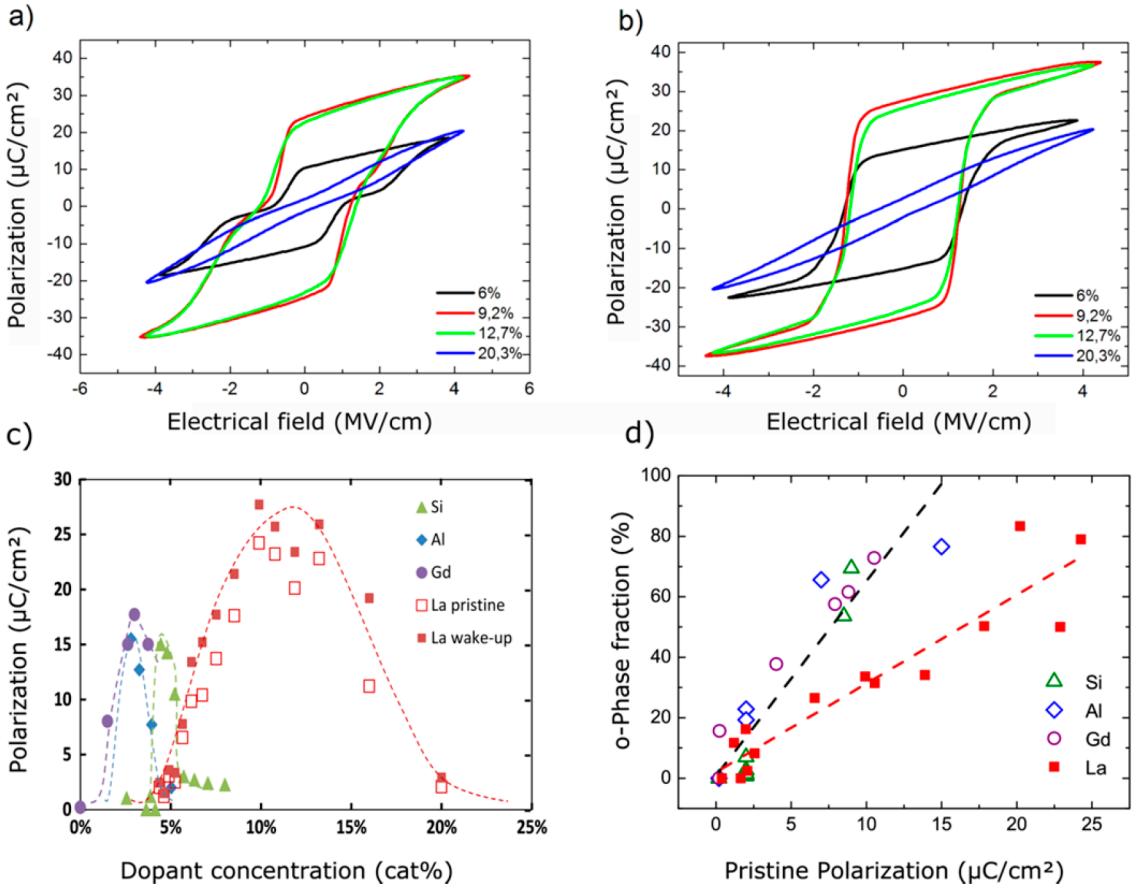

Figure 6. (a) Polarization hysteresis for ∼10 nm thick pristine samples with different La dopant contents from 6 to 20 cat% annealed at 800 °C for 20 s. (b) Polarization hysteresis for samples with different La dopant contents from 6 to 20 cat% after wake up cycling. (c) Remanent polarization P_r values for ∼10 nm thick Si, Al, Gd, and La doped HfO_2 films with different dopant content annealed at 800 °C for 20 s. For La:HfO_2 values for a "pristine" and "after wake up" sample are included. (d) Pristine remanent polarization P_r values as a function of the orthorhombic phase fraction as determined by refinement of GIXRD patterns for samples shown in (c). Lines are a guide.

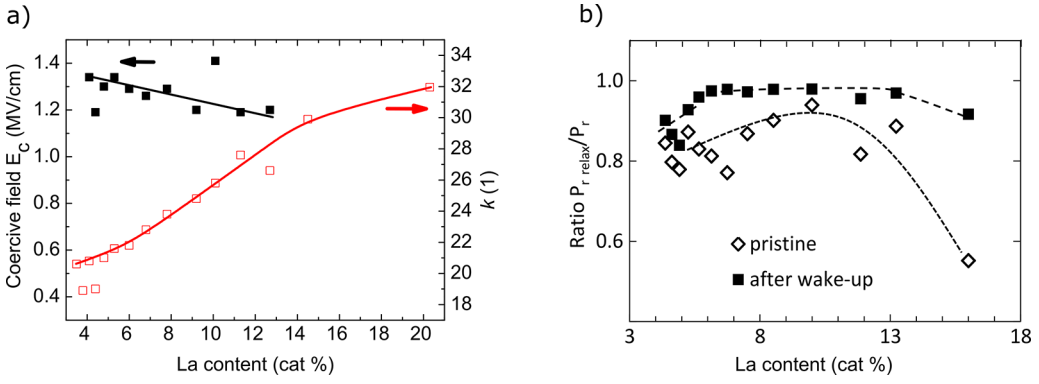

Figure 7. (a) Change of the coercive field E_c (after wake up) and the dielectric constant k for ∼10 nm thick HfO_2 films with different La content. (b) Normalized relaxed remanent polarization after 1 s $P_{r,\,relax}$ (divided by remanent polarization P_r) for different La content for the pristine sample and after wake up cycling. Lines are a guide.

on the pristine samples and after wake up cycling (∼1 × 10^6 field cycles at 100 kHz). Compared to other dopants, ferroelectric properties are observed in a much broader dopant concentration range (Figure 6c) of 12 cat% compared to Si ref 3, Al ref 4, or Gd ref 6 doping with a lower range of 2−4 cat%. Only a mixed $Hf_{1-x}Zr_xO_2$ is showing an even larger window of more than 40 cat%.[5,21] In addition, the region of ferroelectric properties is shifted to higher doping concentrations. For Si, Al, and Gd some ferroelectric properties could be reached starting at ∼2−4 cat%, whereas the lowest La doping showing spontaneous polarization is ∼4−5 cat%. The differences in concentration process window are explained in density functional theory (DFT) simulations by the advantages of La as a dopant caused by the higher ionic radius and improved electronegativity resulting in a dopant oxygen bond length reduction between the dopant cation and the second nearest oxygen neighbor that stabilizes the orthorhombic phase.[11]

Final edited form was published in "Inorganic Chemistry". 2018, 57(5), S. 2752-2765. ISSN 1520-510X.
https://doi.org/10.1021/acs.inorgchem.7b03149

From the structural point of view, a phase transformation from a centrosymmetric nonpolar monoclinic ($P2_1/c$) to a ferroelectric orthorhombic ($Pca2_1$) to a nonpolar cubic phase ($Fm3m$) is characterized by XRD and TEM for increasing La content as described in the previous sections. Parallel to a structural transition a change of the dielectric constant k is expected[37] (see Figure 7). According values are determined by small signal capacitance−voltage measurements indicating an increase of the k value from 20, as expected for mostly monoclinic films,[38] to 28 for the orthorhombic phase,[38] and to 32 for the cubic phase[38] with increasing La content. These results correlate nicely to the measured remanent polarization values. Only in the La dopant range that showed orthorhombic properties in XRD a remanent polarization is detected. Polarization electric field (P E) measurements reveal a clear linear dielectric behavior for a low La content less than 4 cat% La. At 4−5 cat% La the hysteresis loop is opening, and the remanent polarization is steadily increasing to a maximum P_r value of 27.7 μC/cm^2 for 10 cat% La. Beyond 13 cat% La, the P_r value is decreasing again until ∼20 cat%, when almost no ferroelectric properties are visible anymore. In most cases, a pinched hysteresis is visible for pristine samples implying the presence of internal bias fields (Figure 6a).[52] This pinching of the hysteresis disappears during field cycling indicating a reduction of the internal bias (Figure 6b; see also Section 3.4). This effect was described before[39,37] as a nonuniform distribution of oxygen vacancies at the TiN/HfO_2 interface or domain boundaries, which are trap sites that can be charged and likely impact polarization switching and domain pinning. Field cycling could lead to a more equal distribution of these charged O vacancies and thus cause a reduction or disappearance of the internal bias fields. Another explanation would be that vacancy positions and other trap sites are locally fixed and that only a redistribution of trapped electrons cause depinching of the hysteresis. Only for the La:HfO_2 sample with 16 cat% La, a pinched P E loop was measured, which remained during field cycling. Only a slight depinching is visible, which is discussed in more detail in Section 3.4. Accordingly, none of the samples showed a strong field induced ferroelectric behavior as reported for Si and Al doped HfO_2 as well as for a $Hf_xZr_{1-x}O_2$ mixed oxide. Only at 20 cat% La a small field induced hysteresis might be present. Differences to smaller dopants could be related to a change in phase transition. For Si: and Al:HfO_2 and mixed $Hf_xZr_{1-x}O_2$ a transition from the orthorhombic to the tetragonal phase occurs when enhancing the dopant content. For La as for other dopants larger than Hf, a transition to the cubic phase is suggested (see Section 3.2). It is believed that field induced ferroelectric behavior can mainly occur in predominantly tetragonal samples.

A clear linear relation between the o phase fraction and the pristine P_r value is found similar to other dopants like Si, Al, or Gd (Figure 6d) indicating a content independent texture of the film.

Extrapolation of the relation is implying a maximum remanent polarization value of ∼30 μC/cm^2 for a 100% orthorhombic phase fraction. This value is higher than expected for a random orientation of the grains. Theoretical calculations for pure HfO_2 determined a maximum remanent polarization of 50−52 μC/cm^2[40,41] for the orthorhombic HfO_2 phase leading to a P_r value of ∼26 μC/cm^2 for a random grain orientation.[42] XRD results in Section 3.2 suggest a stronger texture of La:HfO_2 in polarization direction, and accordingly a higher remanent polarization value is expected compared to other dopants that create a more random orientation of the HfO_2 grains. The high remanent polarization value also indicates that the film is mainly in the polar orthorhombic $Pca2_1$ phase, and other orthorhombic phases are unlikely. The linear relationship between the phase portions as extracted by Rietveld refinement and the remanent polarization values verify that a refinement can distinguish between different HfO_2 phases especially the orthorhombic and the tetragonal/cubic phase. Deviations from the linear behavior mainly give an indication of the uncertainty of the refinement, since variations of the remanent polarization value for different capacitor structures on the sample are typically below ±1 μC/cm^2. Further analyzing the polarization hysteresis, the coercive field $E_c = (E_{c^+} - E_c)/2$ after wake up is plotted as a function of the La content in the film (Figure 7a). Once a clear polarization hysteresis is measured an almost stable E_c value is revealed, which is slightly dropping from 1.35 MV/cm for 5 cat% La to below 1.2 MV/cm for 13 cat% La in parallel to a k value increase.

The relaxed remanent polarization ($P_{r,\,relax}$) can be measured after 1 s. By comparing $P_{r,relax}$ to P_r, it can be verified if a depolarization field is present in the layer that is reducing the remanent polarization after a certain waiting time. Figure 7b shows $P_{r,relax}$ for the pristine case in comparison to the sample after 1×10^4 field cycles. In the pristine case, only the sample with ∼10 cat% La content exhibits almost no polarization relaxation. This is the La content, where 80% of the film is already in the orthorhombic phase for the pristine sample (see Figure 3c). The depolarization effect is weaker for La contents below 10 cat% when the monoclinic phase portions are present compared to ∼45% relaxation losses for the 16 cat% sample with large cubic phase fractions. This situation is improving drastically after field cycling, where the polarization is very stable, and no relaxation decrease can be detected in a La content range from 7 cat% to 13 cat%. On the basis of TEM analysis, Grimley et al. reported a field cycling induced phase transformation from the monoclinic to the orthorhombic phase for a Gd doped HfO_2 film.[39] Because of the similarities of both dopants (e.g., same valence, comparable ionic radius) a similar phase change during field cycling is expected for La:HfO_2. For 16 cat% La a partial cubic to orthorhombic phase transition is necessary to explain enhancements in the remanent polarization and relaxed polarization value (Figure 7b). Accordingly, the improved polarization relaxation behavior could be an indication that the orthorhombic phase portion is enhanced in this wider La concentration range. One possible root cause could be a more uniform distribution of oxygen vacancies after field cycling, which enhances the oxygen vacancy concentration within the bulk of the HfO_2 film and favors the transformation to the orthorhombic phase.[37]

In addition to the change in polarization relaxation, a broadening of the hysteresis curve (E_c enhancement for positive and negative voltage) and an overall shift of the hysteresis loop to positive voltages during field cycling at room temperature is observed.

A clear improvement of the pinched hysteresis shape is visible for all samples after endurance field cycling, but the process is strongly enhanced for higher monoclinic (<10 cat%) and cubic (>13 cat%) phase portions in the film (Figure 6a; see also Figure SI 4 in Supporting Information). Here, a reduction in the internal bias field as discussed in more detail in the field cycling section is resulting in a depinching of the hysteresis ("broadening"), which can be observed as a change of the intersection of the hysteresis with the x axis. At 5 cat% La

Final edited form was published in "Inorganic Chemistry". 2018, 57(5), S. 2752-2765. ISSN 1520-510X.
https://doi.org/10.1021/acs.inorgchem.7b03149

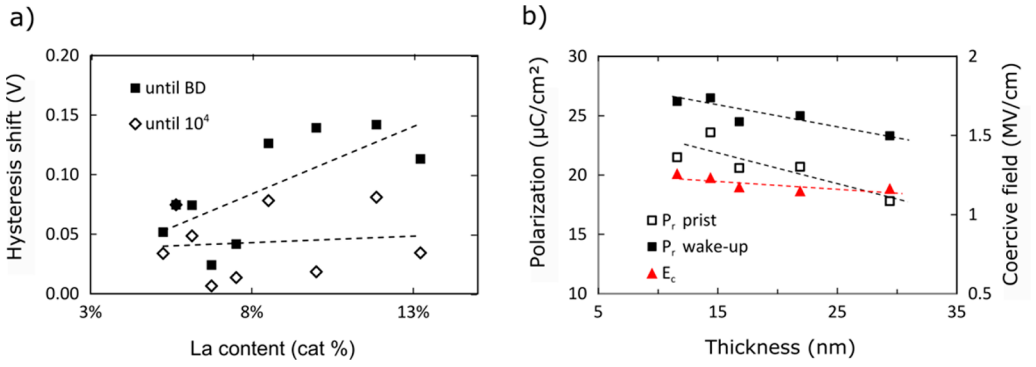

Figure 8. (a) Shift of the hysteresis curve after 1×10^4 field cycles for capacitors with ∼10 nm thick HfO_2 films having different La content and before breakdown compared to the pristine case. (b) Thickness dependence of the remanent polarization P_r for pristine samples (□) and after wake up cycling (■, left axis) and coercive field E_c (▲, right axis) after wake up for La:HfO_2 based capacitor structures with 10 cat% La content. Lines are a guide.

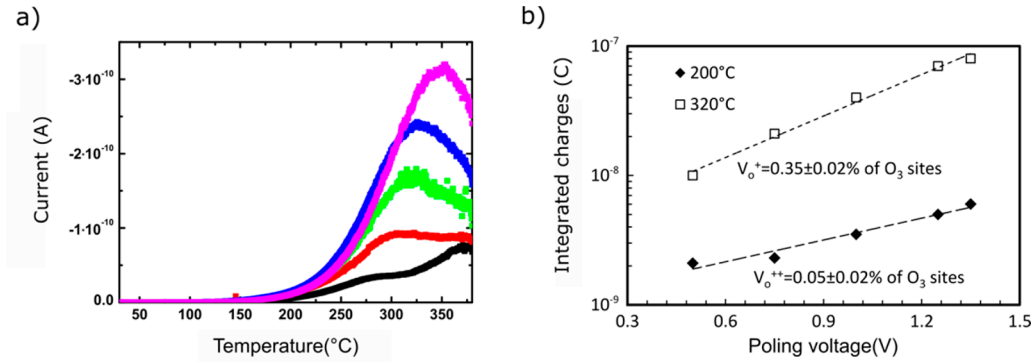

Figure 9. (a) Thermally stimulated depolarization current measurement of 20 nm thick TiN La:HfO_2−TiN capacitors with 10 cat% La after poling with voltages between 0.5 and 1.35 V for 800 s at 380 °C. (b) Extracted charges of the depolarization current measurements using 200 and 320 °C as poling temperatures (see Supporting Information for details).

content an intersection value change up to ±0.4 V is detected, which completely disappears for a La content of more than 10 cat% and increases again for 16 cat% La. This trend is similar for both polarity directions, indicating that only in the La content region between 10 and 13 cat% stable ferroelectric properties exist. This is consistent with a high orthorhombic phase portion in this concentration region. Furthermore, an average shift of the hysteresis along the electric field axis typically descript as imprint (change of the difference between the positive and negative intersection value) of 30 ± 3 mV after 1×10^4 field cycles compared to the pristine case is calculated for all different La/Hf compositions indicating no clear composition dependent behavior (Figure 8a). Since a hysteresis biasing is typically related to charge trapping in the interfacial regions to the electrodes,[43] a stable shift of the hysteresis to a certain positive bias reveals a higher amount of negative charge at the interface to the top electrode, indicating a different interface property at the top and bottom electrodes. Since this shift is already visible at room temperature an even stronger behavior is expected for elevated temperatures. More detailed studies are needed to characterize this behavior. Furthermore, in Figure 8a the voltage shift for the last measurement point before breakdown is plotted as a function of the La content. Since the field cycles to breakdown increase for higher La content, also a stronger voltage shift is expected, assuming the shift is caused by charge trapping during field cycling.[43,44] Indeed this is observed in Figure 8a, where the voltage shift increases from ∼50 to ∼150 mV for samples that are cycled from 1×10^4 to 1×10^9 times, respectively.

So far, detailed electrical characterization is only discussed for 12−14 nm thick La:HfO_2 films. Figure 8b shows the remanent polarization values in a thickness range from 10 to 30 nm La:HfO_2 with 10 cat% La content. The polarization value slightly decreased from 27 $\mu C/cm^2$ for a 10 nm sample to 23 $\mu C/cm^2$ for a 30 nm film. Accordingly, ferroelectric properties are expected for an even wider thickness range.

This trend is similar to Gd:HfO_2 films, but a much stronger reduction of P_r with thickness was observed for smaller dopants like Si and Al,[22] likely caused by the better stabilization properties for La and Gd as predicted through ab initio simulations.[11] For higher film thickness an increase in the monoclinic phase fraction is expected.[22] Within this thickness range the coercive field E_c is stable from 1.1 to 1.2 MV/cm.

For the characterization of defects in the HfO_2 layer, the thermally stimulated depolarization current technique (TSDC) is applied. To identify the responsible charge carriers and trap sites measurements are conducted on a 10 cat% La sample. Initially, the sample is polarized at 380 °C with an applied electric field and rapidly cooled, while the same electric field is still applied to freeze possible diffused charges in their local and energetic positions. Subsequently, during slow heating with 0.2 K/s the depolarization current is measured revealing two current maxima at ∼275 and 320 °C (Figure 9a). For a separation of these peaks, a thermal cleaning method is applied.[45] The measurement of only the relaxation current peak

Final edited form was published in "Inorganic Chemistry". 2018, 57(5), S. 2752-2765. ISSN 1520-510X.
https://doi.org/10.1021/acs.inorgchem.7b03149

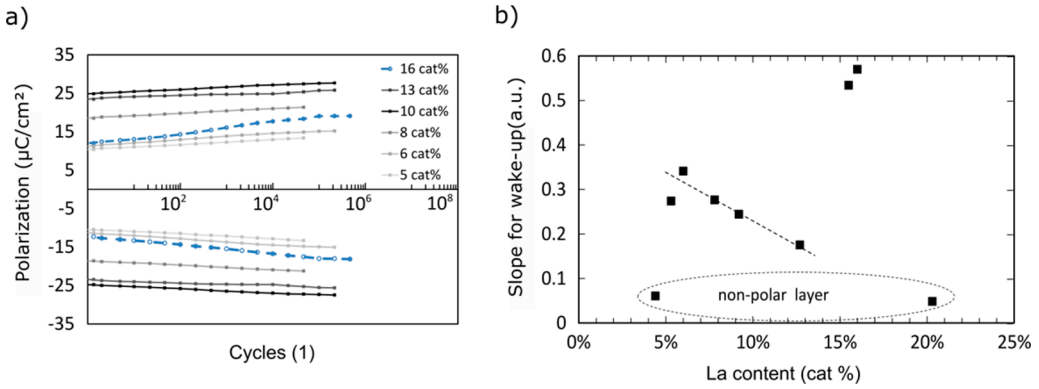

Figure 10. (a) Polarization as a function of electrical field cycling showing the wake up behavior for ~10 nm thick HfO_2 films with different La contents from 5 cat% to 16 cat%. Samples were cycled with rectangular pulses of 4 MV/cm at 100 kHz. (b) Slope of the logarithmic change of the remanent polarization as a function of La content. The lines are a guide.

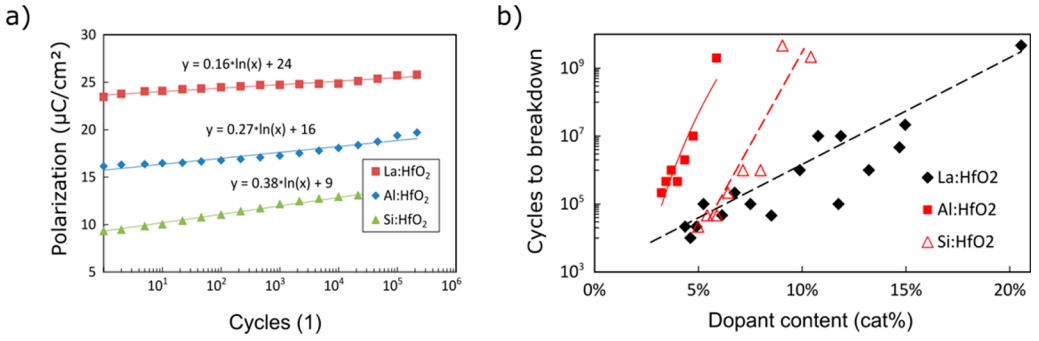

Figure 11. (a) Polarization as a function of electrical field cycling showing the wake up behavior for ~10 nm thick HfO_2 films with La, Al, and Si dopant for samples with the highest remanent polarization value. (b) Cycles to breakdown as a function of the La, Al, and Si dopant concentrations. Lines are a guide.

at 320 °C is achieved by poling the sample at 350 °C and cooling it to 250 °C, while applying the same poling voltage and holding the temperature for 800 s without application of the bias voltage to allow relaxation of charges with lower activation energy (see Figure SI 8a). The current peak at 275 °C is separated by poling only at 200 °C, which does not allow charges with higher activation energy to move (see Figure SI 8b). The activation energies are determined by using the initial rise method[46] as 0.45−0.51 eV (see Figure SI 8c) and 1.23−1.46 eV (see Figure SI 8d) depending on the applied poling voltage. Those values are similar to reported values in literature determined by simulation for singly (1.2 eV)[47] and doubly charged oxygen vacancies (0.7 eV)[47,48] and experimental determined values of 0.51−0.62 eV and 1.06−1.25 eV by TSDC in ferroelectric $Hf_{0.5}Zr_{0.5}O_2$.[50] The voltage dependence of the amount of diffused charges should follow a sinh relation[49]

$$Q_{TSDC} = Q_0 \sinh \frac{eaV_b}{2k_B T_b d}$$

where Q_{TSDC} denotes the charges calculated from integration of the TSDC current peak, e is the elementary charge, a is the valence of the ion, V_b is the used bias voltage, k_B is the Boltzmann constant, and d is the thickness of the film. Similar to a former study[50] this function is fitted to the measurement data to extract the amount of mobile charge carriers per volume for both peaks (see Figure 9b). Values of 0.35% singly and 0.05% doubly charged oxygen vacancies are approximately a factor 2 higher compared to reported values for $Hf_{0.5}Zr_{0.5}O_2$, which might be caused by the lower valence of La compared to Zr.

Another outcome of the former TSDC analysis for $Hf_{0.5}Zr_{0.5}O_2$ was that the hopping frequency was in the millihertz range, which indicated that a low amount of oxygen vacancy diffusion was present at TSDC measurement conditions and that the depolarization current was related to electron hopping.[50] Hence, this suggests that also depinching of the polarization hysteresis during wake up cycling might be caused by movement of trapped electrons in conjunction with field induced phase changes. However, it might still be possible for charged oxygen vacancies to diffuse under much higher applied fields compared to the TSDC measurement conditions in the range of 4 MV/cm even at room temperature.

3.4. Field Cycling Behavior. For the application of ferroelectric doped HfO_2 in a nonvolatile memory cell, the electric field cycling performance of the capacitor structure is of interest. Figure 10a shows the change of the remanent polarization with the number of rectangular electric field cycles (4 MV/cm at 100 kHz). A linear increase of P_r in the semilogarithmic plot is visible for all La concentrations, which is called wake up phase. The slope of this wake up plot in Figure 10a decreases slightly with increasing La content (Figure 10b). For 5 cat% La, a wake up slope of ~0.35 $\mu C/cm^2$ per $\log_{10}$(cycles) is determined, which decreases for higher La concentration, until no wake up is present for the sample with greater than 20 cat% La. Only the sample with a 16 cat% La amount reaches higher values. Here, only cubic phase portions are assumed to be converted to the orthorhombic phase

Final edited form was published in "Inorganic Chemistry". 2018, 57(5), S. 2752-2765. ISSN 1520-510X.
https://doi.org/10.1021/acs.inorgchem.7b03149

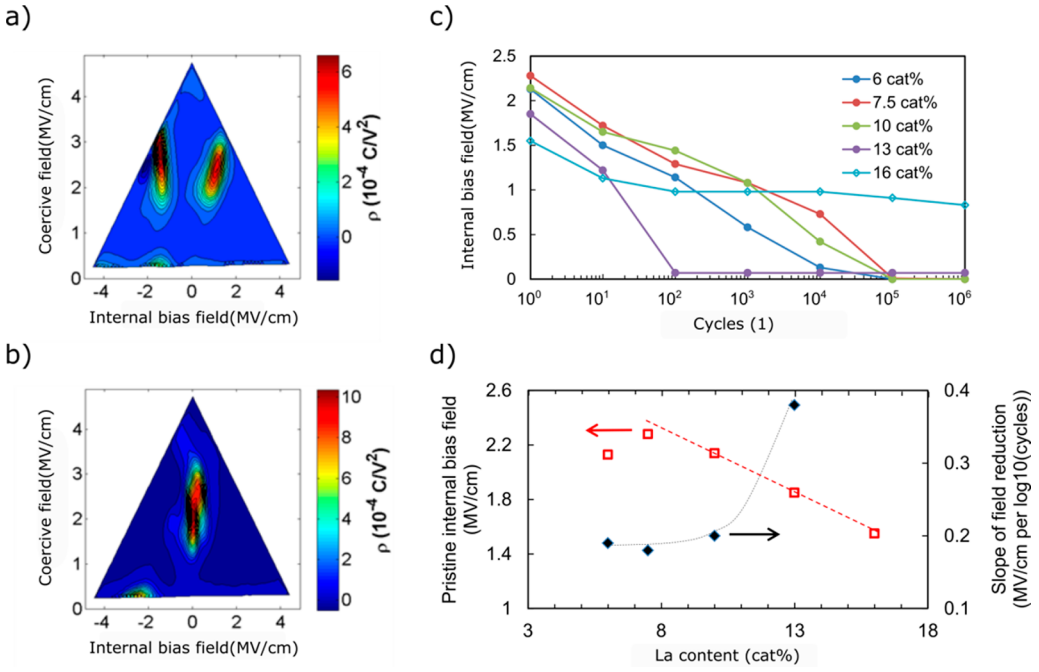

Figure 12. FORC measurement results of ∼10 nm thick HfO_2 films with 10 cat % La content in capacitors (a) before cycling and (b) after 1×10^6 rectangular pulses with 100 kHz at 4 MV/cm. (c) Internal bias field defined as the difference in E_{bias} of the FORC maxima from the pristine and the cycled sample as a function of the number of field cycles. (d) Pristine internal bias field (red □, left axis) and slope m of the decrease in internal bias field $m \times \log_{10}$(cycles) (black ◆, right axis) as extracted from (c). Lines are a guide.

compared to a monoclinic to orthorhombic phase change below 10 cat% La. Above 20 cat% La mainly cubic phase portions are detected (see Figure 3c), and applied electric fields are not able to transform the film into the polar phase. Pešić et al. explained the wake up behavior by field induced oxygen vacancy movement from the electrode interfaces to the HfO_2 bulk causing a phase transformation of nonpolar monoclinic phase portions to the polar orthorhombic phase.[37] Since oxygen vacancy movement could not be confirmed with certainty in the former sections, a pure field driven phase change without oxygen vacancy movement might be an alternative explanation. Similar processes might occur for cubic phase portions for a La content greater than 13 cat%. Since the field drop over the monoclinic domains (with lower dielectric constant) is expected to be higher compared to the one over the cubic domains, a different wake up slope might be expected when a different ion vacancy movement or field driven phase change is assumed in the effective field, resulting in a stronger wake up for monoclinic phase portions containing samples in contrast to cubic counterparts.

Compared to other dopants like Si and Al processed in a similar metal−insulator−metal capacitor structure and using the same TiN electrodes and annealing conditions, La shows a similar wake up slope ranging from 0.2 to 0.4 $\mu C/cm^2$ per decade. However, overall samples with a La content of 13 cat% have the lowest wake up slope as shown in Figure 11a. This behavior indicates less pinching in the pristine case, which suggests that the charge distribution in the highly La doped sample is more uniform, and less domain pinning is present. Higher crystallization anneal temperatures for a 10 cat% La sample improved the wake up properties due to the enhanced orthorhombic phase for annealing temperatures of 800−1000 °C (Figure SI 2).

All samples show a dielectric breakdown after a certain number of field cycles. This hard breakdown event occurs for a higher amount of field cycles with increasing La content (Figure 11b). For 4 cat% La, a low value of $\sim 1 \times 10^3$ cycles is determined compared to 1×10^7 to 1×10^9 cycles to breakdown for samples with more than 10 cat% La. This trend is comparable to other dopants like Si ref 3, Al ref 4, or a mixed $Hf_xZr_{1-x}O_2$[51] oxide. In all cases, the lifetime of the devices improves with higher doping concentration (Figure 11b). Since this trend is always present even though a polarization change is correlated to the phase change from the monoclinic via the orthorhombic to the tetragonal/cubic phase, the lifetime enhancement cannot be related to the remanent polarization value. The phase change with higher dopant content is causing an increase of the dielectric constant of the La:HfO_2 by almost a factor of 2 (Figure 7), interfacial regions with a higher La and Ti content as measured by TOF SIMS (Figure 2b) might have a different dielectric constant compared to the bulk of the film. This means that, for low dopant concentrations, the field within the bulk dielectric would be enhanced by the lower k value promoting an earlier breakdown compared to higher La doping, where the electric field in the bulk might be reduced due to the higher k value.[43] Since a similar dielectric constant increase is visible for different dopants a comparable lifetime enhancement might be expected.

As discussed in the first section, the films are optimized for high remanent polarization values, which are reached by higher annealing temperatures of 800 °C. For nonvolatile memory applications a long lifetime and a high number of endurance cycling is required. As revealed in Figure 1, this enhanced behavior can be achieved by reducing the anneal temperature below 600 °C leading only to a small reduction in remanent polarization values. Further improvements are reported for even lower anneal temperatures and even lower doping concentrations.[12] In former studies on HfO_2 doped with different dopants, an internal bias field is revealed by first order reversal curve (FORC) measurements (details see Experimen

Final edited form was published in "Inorganic Chemistry". 2018, 57(5), S. 2752-2765. ISSN 1520-510X.
https://doi.org/10.1021/acs.inorgchem.7b03149

tal Section) on pristine samples that decreased during field cycling.[52] As a model, a redistribution of charges[37] from the TiN electrode interfaces toward the HfO_2 bulk and within the interface and domain boundary regions is suggested. As discussed in the beginning of the Electrical Characterization section, these charges can pin domains, thus causing a pinched hysteresis loop.

During field cycling, a redistribution of charges at trap sites (e.g., oxygen vacancies) within the HfO_2 could lead to a phase transformation and more uniform distribution of pinning centers, which consequently results in the opening of the hysteresis (Figure 12a).[37] Similar to previous investigations on HfO_2 based materials,[52,53] FORC measurements are performed on HfO_2 samples with different La content ranging from 6 to 16 cat%. In all cases, a reduction of the internal bias field (defined as the difference in E_{bias} of both FORC maxima) with field cycling is verified (Figure 12a−c). The initial value decreases from ∼2.4 MV/cm for 7.5 cat% to 1.6 MV/cm for 16 cat% La. These E_{bias} values follow an exponential reduction with the number of cycles $E_{bias} \approx -m \cdot \log_{10}(\text{cycles})$, resulting in a vanishing of the internal bias field after 1×10^6 field cycles for all samples except the 16 cat% case. The slope m improves from 0.16 to 0.38 MV/cm per decade with higher La content below 13 cat%, similar to the improvement in wake up behavior with increasing La content, as discussed in the beginning of this section. Again, only the sample with 16 cat% La is not following the general trend. The internal bias field of 1.5 MV/cm is lower for the pristine sample with 16 cat% and changes much less with cycling (slope $m \approx 0.2$ MV/cm per decade). The linear reduction of the internal bias field (Figure 12d) with increasing La content could be related to a reduced amount of trap sites with enhanced La concentration, which would not be expected for a higher amount of trivalent La in HfO_2. A lower amount of trap sites would improve the wake up behavior as indicated by the slope for field reduction. As mentioned before, only for samples with significant cubic portions the wake up behavior is modified. Overall, the distribution of the coercive field as determined by the FORC method during cycling is almost constant with a mean value of 2.3 ± 0.5 MV/cm. This value is higher than results reported in Figure 7, which is caused by a higher effective measurement frequency to avoid sample degradation during FORC measurement. For FORC plots, an effective frequency of 16 kHz is used with respect to 1 kHz used in the PE measurement as described in Figure 7. Variations of the coercive field are discussed to be related to the distribution in grain sizes by Hoffmann et al.[22]

Comparing structural and electrical results, the following trends are visible. La shows an almost uniform dopant distribution within the HfO_2 bulk, with the exception of an enrichment at the oxide/TiN electrodes interfaces. Former studies[22,23] revealed an interfacial reaction during crystallization anneal of the capacitor stack, which results in O diffusion into the TiN and Ti/N diffusion into the HfO_2 interfacial regions causing a higher amount of oxygen vacancies at these interfaces. A similar behavior could be verified in the TOF SIMS analysis indicating a clear TiO_x interface formation similar to reports for Gd:HfO_2.[22] Hereby generated oxygen vacancies can act as trap sites, which can be singly and doubly charged with a trap depth of 0.5 and 1.1 eV similar to other dopants.[50] Higher La amounts seem to reduce the oxygen vacancy content and improve the uniformity throughout the HfO_2 bulk, because wake up and breakdown behavior of the layer is improved. On the one hand, a constant imprint behavior for different La concentrations indicates a similar interfacial trap concentration, since this shift is typically caused by charging of interfacial traps during field cycling. Furthermore, comparing all electrical parameters, anneal temperatures of ∼800 °C are necessary to enhance the orthorhombic phase portion in the layer to a fraction close to 90% and to enable low wake up and low relaxation behavior to ensure long polarization retention. On the other hand, lower annealing temperatures are preferred to avoid defect diffusion from the TiN electrodes into the HfO_2 layer and to optimize breakdown, endurance, and internal bias fields, accordingly. Since back end capacitors require low maximum anneal temperatures of 400−500 °C, a compromise must be found to optimize the device performance. La Doped HfO_2 layers have the advantage of a broad dopant range, which enables easier device tuning, but here higher crystallization temperatures compared to $Hf_xZr_{1-x}O_2$ are disadvantageous. For transistor applications, an optimized material performance at higher anneal temperatures as shown for La:HfO_2 can be beneficial.

4. SUMMARY

Ferroelectric properties of La doped HfO_2 are reported in a wide dopant concentration range of ∼12 cat%, which is broader compared to other dopants, which typically only have a 2−3 cat % window. Only mixed $Hf_xZr_{1-x}O_2$ oxides reach an even higher concentration range for ferroelectricity. Because of this enhanced process window a film consisting almost exclusively of the non centrosymmetric polar orthorhombic phase is fabricated, which exhibits low depolarization fields and accordingly minimal polarization relaxation. These results support predictions of ab inito calculations indicating an improved stabilization of the ferroelectric orthorhombic phase caused by dopants with larger ionic radius and lower electronegativity leading to an additional metal−oxygen bond. Interfacial trap sites at oxygen vacancies caused by a local reaction of La:HfO_2 with the TiN electrodes are determined to be the main reason for the observed internal bias fields in pristine samples. These bias fields disappear during electric field cycling due to a redistribution of charges. Furthermore, high remanent polarization values $2P_r$ of 55 $\mu C/cm^2$ are determined caused by a prominent texture of the orthorhombic phase in the (002) direction. For best field cycling behavior a La doping level of 10−13 cat% results in longer device lifetimes up to 1×10^7 field cycles (4 MV/cm at 100 kHz), and lower wake up behavior indicated by a reduced wake up slope. This improve ment in wake up with field cycling is assigned to a reduction in internal bias fields due to a redistribution of charges. Field cycling is also causing partial phase changes from the monoclinic and cubic to the orthorhombic phase. Here, the phase change from the monoclinic phase to the orthorhombic phase seems to occur much faster compared to the phase change starting with the cubic phase.

■ ASSOCIATED CONTENT

Additional structural data concerning the polycrystalline nature of lanthanum doped ferroelectric hafnium oxide in a capacitor structure with titanium nitride electrodes

Final edited form was published in "Inorganic Chemistry". 2018, 57(5), S. 2752-2765. ISSN 1520-510X.
https://doi.org/10.1021/acs.inorgchem.7b03149

(XRD, SEM, TEM, TOFSIMS) and more figures concerning detailed electrical characterization (PDF)

AUTHOR INFORMATION

Corresponding Author

*E mail: uwe.schroeder@namlab.com.

ORCID

Uwe Schroeder: 0000 0002 6824 2386
Min Hyuk Park: 0000 0001 6333 2668
Tony Schenk: 0000 0003 2933 1076
Michael Hoffmann: 0000 0001 6493 3457
Thomas Mikolajick: 0000 0003 3814 0378

Author Contributions

The manuscript was written through contributions of all authors. All authors have given approval to the final version of the manuscript.

Notes

The authors declare no competing financial interest.

ACKNOWLEDGMENTS

Authors gratefully acknowledge E. Grimley for intensive discussion and T. Sturm and A. Poehl from Leibniz IFW Dresden, Germany, for preparing the TEM lamella. This work was supported in part by funding from Army Research Office (Contract No. W911NF 15 1 0593). T.S. gratefully acknowl edges the German Research Foundation (Deutsche For schungs Gemeinschaft) for funding part of this research in the frame of the "Inferox" project (MI 1247/11 2). M.P. and C.R. are supported by the EFRE fund of the European Commission and by the Free State of Saxony (Germany). M.H.P. is supported by Humboldt postdoctoral fellowship from Alexander von Humboldt Foundation. This work was performed in part at the Analytical Instrumentation Facility (AIF) at North Carolina State Univ., which is supported by the State of North Carolina and the National Science Foundation (Award No. ECCS 1542015). The AIF is a member of the North Carolina Research Triangle Nanotechnology Network (RTNN), a site in the National Nanotechnology Coordinated Infrastructure (NNCI). M.H. has received funding from the Electronic Component Systems for European Leadership Joint Undertaking under Grant No. 692519. This Joint Undertaking receives support from the European Union Horizon 2020 research and innovation program and Belgium, Germany, France, Netherlands, Poland, and United Kingdom.

REFERENCES

(1) Ihlefeld, J. F.; Harris, D. T.; Keech, R.; Jones, J. L.; Maria, J. P.; Trolier McKinstry, S. Scaling Effects in Perovskite Ferroelectrics: Fundamental Limits and Process Structure Property Relations. *J. Am. Ceram. Soc.* **2016**, *99* (8), 2537−2557.

(2) Böscke, T. S.; Müller, J.; Bräuhaus, D.; Schröder, U.; Böttger, U. Ferroelectricity in hafnium oxide thin films. *Appl. Phys. Lett.* **2011**, *99*, 102903.

(3) Richter, C.; Schenk, T.; Park, M. H.; Tscharntke, F. A.; Grimley, E. D.; LeBeau, J. M.; Zhou, C.; Fancher, C. M.; Jones, J. L.; Mikolajick, T.; Schroeder, U. Si Doped Hafnium Oxide—A "Fragile" Ferroelectric System. *Adv. Electron. Mater.* **2017**, *3*, 1700131.

(4) Mueller, S.; Mueller, J.; Singh, A.; Riedel, S.; Sundqvist, J.; Schroeder, U.; Mikolajick, T. Incipient Ferroelectricity in Al Doped HfO_2 Thin Films. *Adv. Funct. Mater.* **2012**, *22*, 2412.

(5) Müller, J.; Böscke, T. S.; Bräuhaus, D.; Schröder, U.; Böttger, U.; Sundqvist, J.; Kücher, P.; Mikolajick, T.; Frey, L. Ferroelectric $Zr_{0.5}Hf_{0.5}O_2$ thin films for nonvolatile memory Applications. *Appl. Phys. Lett.* **2011**, *99*, 112901.

(6) Mueller, S.; Adelmann, C.; Singh, A.; Van Elshocht, S.; Schroeder, U.; Mikolajick, T. Ferroelectricity in Gd Doped HfO_2 Thin Films. *ECS J. Solid State Sci. Technol.* **2012**, *1*, N123.

(7) Kozodaev, M. G.; Chernikova, A. G.; Korostylev, E. V.; Park, M. H.; Schroeder, U.; Hwang, C. S.; Markeev, A. M. Ferroelectric properties of lightly doped La:HfO2 thin films grown by plasma assisted atomic layer deposition. *Appl. Phys. Lett.* **2017**, *111*, 132903.

(8) Schenk, T.; Mueller, S.; Schroeder, U.; Materlik, R.; Kersch, A.; Popovici, M.; Adelmann, C.; Van Elshocht, S.; Mikolajick, T. Strontium Doped Hafnium Oxide Thin Films: Wide Process Window for Ferroelectric Memories. ESSDERC 2013, *Proc. Eur. Solid State Device Res. Conf., 43rd*, 2013, 260−263 10.1109/ESSDERC.2013.6818868.

(9) Schroeder, U.; Yurchuk, E.; Müller, J.; Martin, D.; Schenk, T.; Polakowski, P.; Adelmann, C.; Popovici, M. I.; Kalinin, S. V.; Mikolajick, T. Impact of different dopants on the switching properties of ferroelectric hafniumoxide. *Jpn. J. Appl. Phys.* **2014**, *53*, 08LE02.

(10) Sang, X.; Grimley, E. D.; Schenk, T.; Schroeder, U.; LeBeau, J. M. On the structural origins of ferroelectricity in HfO_2 thin films. *Appl. Phys. Lett.* **2015**, *106*, 162905.

(11) Batra, R.; Doan Huan, T.; Rossetti, G. A., Jr.; Ramprasad, R. Dopants Promoting Ferroelectricity in Hafnia: Insights from a comprehensive Chemical Space Exploration. *Chem. Mater.* **2017**, *29*, 9102.

(12) Kozodaev, M. G.; Chernikova, A. G.; Korostylev, E. V.; Park, M. H.; Schroeder, U.; Hwang, C. S.; Markeev, A. M. Ferroelectric properties of lightly doped La:HfO_2 thin films grown by plasma assisted atomic layer deposition. *Appl. Phys. Lett.* **2017**, *111*, 132903.

(13) Müller, J.; Boescke, T. S.; Müller, S.; Yurchuk, E.; Polakowski, P.; Paul, J.; Martin, D.; Schenk, T.; Khullar, K.; Kersch, A.; Weinreich, W.; Riedel, S.; Seidel, K.; Kumar, A.; Arruda, T. M.; Kalinin, S. V.; Schlösser, T.; Boschke, R.; van Bentum, R.; Schröder, U.; Mikolajick, T. Ferroelectric Hafnium Oxide: A CMOS compatible and highly scalable approach to future ferroelectric memories. *IEEE Int. Electron Devices Meet.* 2013, 10.8.1 10.8.110.1109/IEDM.2013.6724605.

(14) Chernikova, A. G.; Kuzmichev, D. S.; Negrov, D. V.; Kozodaev, M. G.; Polyakov, S. N.; Markeev, A. M. Ferroelectric properties of full plasma enhanced ALD TiN/La:HfO_2/TiN stacks. *Appl. Phys. Lett.* **2016**, *108*, 242905.

(15) Richter, C.; Schenk, T.; Schroeder, U.; Mikolajick, T. Film properties of low temperature HfO_2 grown with H_2O, O_3, or remote O_2 plasma. *J. Vac. Sci. Technol., A* **2014**, *32*, 01A117.

(16) Niinisto, J. Ph.D. Dissertation, Helsinki University of Technology, 2006.

(17) Park, M. H.; Schenk, T.; Fancher, C. M.; Grimley, E. D.; Zhou, C.; Richter, C.; LeBeau, J. M.; Jones, J. L.; Mikolajick, T.; Schroeder, U. A Comprehensive Study on the Structural Evolution of HfO_2 Thin Films Doped with Various Dopants. *J. Mater. Chem. C* **2017**, *5*, 4677−4690.

(18) Schenk, T. Ph.D. Thesis, TU Dresden, 2017.

(19) Waser, R.; et al. *Nanoelectronics and Information Technology, Capacitor Based Random Access Memories,* 3rd ed.; Wiley VCH, 2012.

(20) Hoffmann, M.; Schenk, T.; Kulemanov, I.; Adelmann, C.; Popovici, M.; Schroeder, U.; Mikolajick, T. Low Temperature Compatible Hafnium Oxide Based Ferroelectrics. *Ferroelectrics* **2015**, *480*, 16−23.

(21) Park, M. H.; Kim, H. J.; Kim, Y. J.; Lee, W.; Kim, H. K.; Hwang, C. S. Effect of forming gas annealing on the ferroelectric properties of $Hf_{0.5}Zr_{0.5}O_2$ thin films with and without Pt electrodes. *Appl. Phys. Lett.* **2013**, *102*, 112914.

(22) Hoffmann, M.; Schroeder, U.; Schenk, T.; Shimizu, T.; Funakubo, H.; Sakata, O.; Pohl, D.; Drescher, M.; Adelmann, C.; Materlik, R.; Kersch, A.; Mikolajick, T. Stabilizing the ferroelectric phase in doped hafnium oxide. *J. Appl. Phys.* **2015**, *118*, 072006.

(23) Weinreich, W.; Reiche, R.; Lemberger, M.; Jegert, G.; Müller, J.; Wilde, L.; Teichert, S.; Heitmann, J.; Erben, E.; Oberbeck, L.; Schroeder, U.; Bauer, A. J.; Ryssel, H. Impact of interface variations on

J−V and C−V polarity asymmetry of MIM capacitors with amorphous and crystalline $Zr_{(1-x)}Al_xO_2$ films. *Microelectron. Eng.* **2009**, *86*, 1826.
(24) Gao, Y. A new secondary ion mass spectrometry technique for III V semiconductor compounds using the molecular ions CsM^+. *J. Appl. Phys.* **1988**, *64*, 3760.
(25) Shimizu, T.; Katayama, K.; Funakubo, H. Epitaxial Growth of $YO_{1.5}$ Doped HfO_2 films on (100) YSZ Substrate with Various Concentrations. *Ferroelectrics* **2017**, *512*, 105−110.
(26) Shiraishi, T.; Katayama, K.; Yokouchi, T.; Shimizu, T.; Oikawa, T.; Sakata, O.; Uchida, H.; Imai, Y.; Kiguchi, T.; Konno, T. J.; Funakubo, H. Impact of mechanical stress on ferroelectricity in $(Hf_{0.5}Zr_{0.5})O_2$ thin films. *Appl. Phys. Lett.* **2016**, *108*, 262904.
(27) Lee, C. K.; Cho, E.; Lee, H. S.; Hwang, C. S.; Han, S. First principles study on doping and phase stability of HfO_2. *Phys. Rev. B: Condens. Matter Mater. Phys.* **2008**, *78*, 012102.
(28) Duran, P. Phase relationships in the systems HfO_2 La_2O_3 and HfO_2 Nd_2O_3. *Ceramurgia Int.* **1975**, *1*, 10.
(29) Komissarova, L. N.; Wang, K. S.; Spitzyn, V. I.; Simanov, Y. P. The HfO_2 La_2O_3 System. *Russ. J. Inorg. Chem.* **1964**, *9*, 383−386.
(30) Shannon, R. D. Revised effective ionic radii and systematic studies of interatomic distances in halides and chalcogenides. *Acta Crystallogr., Sect. A: Cryst. Phys., Diffr., Theor. Gen. Crystallogr.* **1976**, *32*, 751−767.
(31) Macherauch, E. X ray stress analysis. *Exp. Mech.* **1966**, *6*, 140.
(32) Noyan, I. C.; Huang, T. C.; York, B. R. Residual stress/strain analysis in thin films by X ray diffraction. *Crit. Rev. Solid State Mater. Sci.* **1995**, *20*, 125−177.
(33) Dole, S. L.; Hunter, O.; Wooge, C. J. Elastic properties of monoclinic hafnium oxide at room temperature. *J. Am. Ceram. Soc.* **1977**, *60*, 488−490.
(34) Nino, J. C.; Qiu, W.; Jones, J. L. Strain state of bismuth zinc niobate pyrochlore thin films. *Thin Solid Films* **2009**, *517*, 4325−4328.
(35) Böscke, T. S.; Teichert, St.; Bräuhaus, D.; Müller, J.; Schröder, U.; Böttger, U.; Mikolajick, T. Phase transitions in ferroelectric silicon doped hafnium oxide. *Appl. Phys. Lett.* **2011**, *99*, 112904.
(36) Park, M. H.; Schenk, T.; Richter, C.; Grimley, E. D.; LeBeau, J. M.; Tallarida, M.; Mariani, C.; Simonelli, L.; Fancher, C. M.; Jones, J. L.; Materlik, R.; Künneth, C.; Kersch, A.; Mikolajick, T.; Schroeder, U. Structural Root Causes of Ferroelectricity in Doped Hafnium Oxide. In *International Symposium on Applications of Ferroelectrics (ISAF);* Darmstadt, Germany, Aug 21−25, 2016; IEEE, 2016.
(37) Pešić, M.; Fengler, F. P. G.; Larcher, L.; Padovani, A.; Schenk, T.; Grimley, E. D.; Sang, X.; LeBeau, J. M.; Slesazeck, S.; Schroeder, U.; Mikolajick, T. Physical Mechanisms behind the Field Cycling Behavior of HfO_2 Based Ferroelectric Capacitors. *Adv. Funct. Mater.* **2016**, *26*, 4601−4612.
(38) Materlik, R.; Künneth, C.; Kersch, A. The origin of ferroelectricity in Hf1−xZrxO2: A computational investigation and a surface energy model. *J. Appl. Phys.* **2015**, *117*, 134109.
(39) Grimley, E. D.; Schenk, T.; Sang, X.; Pešic, M.; Schroeder, U.; Mikolajick, T.; LeBeau, J. M. Structural Changes Underlying Field Cycling Phenomena in Ferroelectric HfO_2 Thin Films. *Adv. Electron. Mater.* **2016**, *2*, 1600173.
(40) Clima, S.; Wouters, D. J.; Adelmann, C.; Schenk, T.; Schroeder, U.; Jurczak, M.; Pourtois, G. Identification of the ferroelectric switching process and dopant dependent switching properties in orthorhombic HfO_2: A first principles insight. *Appl. Phys. Lett.* **2014**, *104*, 092906.
(41) Materlik, R.; Künneth, C.; Kersch, A. The origin of ferroelectricity in Hf1−xZrxO2: A computational investigation and a surface energy model; *J. Appl. Phys.* **2015**, *117*, 134109.
(42) Jones, J. L. The effect of crystal symmetry on the maximum polarization of polycrystalline ferroelectric materials. *Mater. Sci. Eng., B* **2010**, *167* (1), 6−11.
(43) Pešić, M.; Fengler, F.; Slesazeck, S.; Schroeder, U.; Mikolajick, T.; Larcher, L.; Padovani, A. Root cause of degradation in novel HfO_2 based ferroelectric memories. In *2016 IEEE International Reliability Physics Symposium (IRPS);* Pasadena, CA, Apr 17−21, 2016; 10.1109/IRPS.2016.7574619.
(44) Pešić, M.; Slesazeck, S.; Mikolajick, T.; Schroeder, U. Anti ferroelectric like ZrO_2 non volatile memory: Inducing non volatility within state of the art DRAM. *17th Non Volatile Memory Technology Symposium (NVMTS);* Aachen, Germany, Aug 30−Sept 1, 2017; IEEE, 2017.
(45) Mano, J. F. Modelling of thermally stimulated depolarization current peaks obtained by global and thermal cleaning experiments. *J. Phys. D: Appl. Phys.* **1998**, *31*, 2898.
(46) Liu, W.; Randall, C. A. Thermally Stimulated Relaxation in Fe Doped $SrTiO_3$ Systems: I. Single Crystals. *J. Am. Ceram. Soc.* **2008**, *91*, 3245−3250.
(47) Morozov, M. I.; Damjanovic, D. Charge migration in $Pb(Zr,Ti)O_3$ ceramics and its relation to ageing, hardening, and softening. *J. Appl. Phys.* **2010**, *107*, 034106.
(48) Capron, N.; Broqvist, P.; Pasquarello, A. Migration of oxygen vacancy in HfO_2 and across the HfO_2/SiO_2 interface: A first principles investigation. *Appl. Phys. Lett.* **2007**, *91* (19), 192905.
(49) Hino, T. Thermally Stimulated Characteristics in Solid Dielectrics. *IEEE Trans. Electr. Insul.* **1980**, *EI 15*, 301.
(50) Fengler, F. P. G.; Nigon, R.; Muralt, P.; Grimley, E. D.; Sang, X.; Sessi, V.; Hentschel, R.; LeBeau, J. M.; Mikolajick, T.; Schroeder, U. Analysis of performance instabilities of hafnia based ferroelectrics using modulus spectroscopy and thermally stimulated depolarization currents. *Adv. Electr. Mater.* **2018**, 1700547.
(51) Mittmann, T.; Fengler, F. P. G.; Richter, C.; Park, M. H.; Mikolajick, T.; Schroeder, U. Optimizing process conditions for improved $Hf_{1-x}Zr_xO_2$ ferroelectric capacitor performance. *Micro electron. Eng.* **2017**, *178*, 48−51.
(52) Schenk, T.; Hoffmann, M.; Ocker, J.; Pesic, M.; Mikolajick, T.; Schroeder, U. Complex Internal Bias Fields in Ferroelectric Hafnium Oxide. *ACS Appl. Mater. Interfaces* **2015**, *7*, 20224−20233.
(53) Hoffmann, M.; Schenk, T.; Pešić, M.; Schroeder, U.; Mikolajick, T. Insights into antiferroelectrics from first order reversal curves. *Appl. Phys. Lett.* **2017**, *111*, 182902.